

A. BOGAERTS<sup>1,✉</sup>  
M. GROZEVA<sup>2</sup>

# Effect of helium/argon gas ratio in a He-Ar-Cu<sup>+</sup> IR hollow-cathode discharge laser: modeling study and comparison with experiments

<sup>1</sup> University of Antwerp, Department of Chemistry, Universiteitsplein 1, 2610 Wilrijk-Antwerp, Belgium

<sup>2</sup> Institute of Solid State Physics, Bulgarian Academy of Sciences, 72 Tzarigradsko Chaussee, 1784 Sofia, Bulgaria

Received: 14 October 2002/

Revised version: 28 November 2002

Published online: 19 March 2003 • © Springer-Verlag 2003

**ABSTRACT** The He-Ar-Cu<sup>+</sup> IR laser operates in a hollow-cathode discharge, typically in a mixture of helium with a few-% Ar. The population inversion of the Cu<sup>+</sup> ion levels, responsible for laser action, is attributed to asymmetric charge transfer between He<sup>+</sup> ions and sputtered Cu atoms. The Ar gas is added to promote sputtering of the Cu cathode. In this paper, a hybrid modeling network consisting of several different models for the various plasma species present in a He-Ar-Cu hollow-cathode discharge is applied to investigate the effect of Ar concentration in the gas mixture on the discharge behavior, and to find the optimum He/Ar gas ratio for laser operation. It is found that the densities of electrons, Ar<sup>+</sup> ions, Ar<sub>m</sub><sup>\*</sup> metastable atoms, sputtered Cu atoms and Cu<sup>+</sup> ions increase upon the addition of more Ar gas, whereas the densities of He<sup>+</sup> ions, He<sub>2</sub><sup>+</sup> ions and He<sub>m</sub><sup>\*</sup> metastable atoms drop considerably. The product of the calculated Cu atom and He<sup>+</sup> ion densities, which determines the production rate of the upper laser levels, and hence probably also the laser output power, is found to reach a maximum around 1–5 % Ar addition. This calculation result is compared to experimental measurements, and reasonable agreement has been reached.

PACS 52.65.-y; 52.65.Ww; 42.55.L

## 1 Introduction

One of the main applications of hollow-cathode discharge (HCD) plasmas is in laser technology [1, 2]. In so-called “metal-vapor ion lasers” the metal vapor is commonly produced by the sputtering of the cathode material. Population inversion, necessary for laser action, is obtained for the ionic levels of the metal vapor, most typically by asymmetric charge transfer between the buffer gas ions and the metal vapor atoms. In this work, we focus on a He-Ar-Cu<sup>+</sup> HCD laser, with the most intense laser line at 780.78 nm. The upper and lower laser levels are the  $3d^9 6s^3 D_3$  level and the  $3d^9 5p^3 F_4$  level, respectively. Population inversion of these levels is attributed to asymmetric charge transfer between He<sup>+</sup> ions and

sputtered Cu ground-state atoms. However, helium ions and atoms do not give rise to efficient sputtering due to their low mass. Therefore, Ar is sometimes added to the He HCD [3–9] to promote the sputtering and hence to increase the sputtered ground-state atom density [8]. However, too much Ar addition reduces the production rate of the He<sup>+</sup> ions, because of the lower ionization potential and higher ionization cross section of Ar [4]. A He-Ar pressure ratio of 20 : 1 was experimentally found to give optimum laser conditions [4]. However, in [9], an argon partial pressure of 1 mbar was reported to be optimum, independent of the helium partial pressure and discharge current. The optimum He pressure was found to be about 25 mbar, dependent on the discharge current [9].

In a previous paper [10], we developed a comprehensive hybrid modeling network for a He-Ar-Cu HCD. This modeling network will be applied in the present paper to investigate the effect of Ar addition on various plasma parameters, and to estimate the optimum He/Ar gas ratio for laser operation. This calculation result will also be compared with experimental measurements.

## 2 Description of the model

The hybrid modeling network consists of a number of Monte Carlo and fluid models to describe the behavior of the various plasma species in a He-Ar-Cu HCD. Briefly, the Monte Carlo method is applied for the fast plasma species, which are not in equilibrium with the electric field, i.e. they gain more energy from the electric field than they lose by collisions. The fluid approach, in contrast, is used to treat the behavior of the slow plasma species, which can be considered to be in equilibrium with the electric field.

For the He and Ar gas atoms, no specific model is used, and they are simply assumed to be uniformly distributed in the plasma, assuming a gas temperature of 1000 K. The actual value of the gas temperature is unknown, but a value of 1000 K is expected, based on results of a heat-transfer model for similar conditions [11]. Moreover, the exact value assumed for the gas temperature is not so important because it would only affect the absolute values of the densities and not the qualitative behavior as a function of argon addition.

✉ Fax: +32-3/820-23-76, E-mail: annemie.bogaerts@ua.ac.be

The electrons are split up into two groups, depending on their energy. The fast electrons, i.e. with total (= sum of potential and kinetic) energy above the threshold for inelastic collisions, are treated with a Monte Carlo model. Their trajectory during successive time-steps is calculated by Newton's laws, and the collisions during these time-steps (i.e. occurrence of a collision, the kind of collision and new energy and direction after collision) are treated with random numbers. The collisions taken into account are elastic collisions with He and Ar gas atoms, ionization and excitation of He and Ar ground-state atoms and metastable atoms (denoted throughout this paper as  $\text{He}_m^*$  and  $\text{Ar}_m^*$ ), and ionization of the sputtered Cu atoms. When the total (i.e. the sum of kinetic and potential) energy drops below the threshold for inelastic collisions (i.e. 1.8 eV, for excitation from the  $\text{Ar}_m^*$  metastable level), the electrons are transferred to the slow-electron group. Since these electrons cannot give rise to inelastic collisions anymore, their only role in the plasma is to provide negative space charge and to carry the electrical current. Hence, their behavior is described with a fluid model.

Beside the slow electrons, this fluid model also handles the helium and argon ions. Not only are  $\text{He}^+$  and  $\text{Ar}^+$  ions taken into account, but also the  $\text{He}_2^+$  and  $\text{Ar}_2^+$  ions, which come into play at the relatively high pressure (several torr) and electrical current (several amps) typical for HCD lasers [12, 13]. These ions and electrons are described with a set of continuity and transport equations (one of each for every type of species). The continuity equations contain different production and loss terms, and the transport equations consist of a diffusion term and a migration term in the electric field. These equations are coupled to Poisson's equation to obtain a self-consistent electric field distribution (i.e. the electric field used to calculate the transport of the ions and electrons is calculated self-consistently from the densities of these charged species).

The  $\text{He}^+$  and  $\text{Ar}^+$  ions are not only treated with a fluid model; they are also treated with a Monte Carlo algorithm, which calculates, amongst others, the flux energy distributions of the ions when bombarding the cathode. Note that the flux energy distribution means the energy distribution expressed in terms of the flux, i.e. by integrating over all energies, the total flux is obtained. This flux energy distribution is needed to compute the flux of sputtered Cu atoms (see below). For the  $\text{He}_2^+$  and  $\text{Ar}_2^+$  ions, no Monte Carlo model is applied, because they are still of minor importance than the singly charged ions, and therefore their contribution to sputtering can in the first approximation be neglected.

The Monte Carlo method is, however, also used for the fast He and Ar atoms, created from elastic collisions of the  $\text{He}^+$  and  $\text{Ar}^+$  ions with He and Ar gas atoms. Indeed, because the fast He and (especially) Ar atoms are expected to play a non-negligible role in the sputtering process, it is important to calculate their flux energy distribution as well.

The behavior of the  $\text{He}_m^*$  and  $\text{Ar}_m^*$  metastable atoms is described with two fluid models, which consist of a continuity equation with several production and loss terms, and a transport equation. We consider only one effective  $\text{He}_m^*$  level and one effective  $\text{Ar}_m^*$  level.

As mentioned above, the flux of sputtered Cu atoms is calculated from the flux energy distributions of the bombarding ions and atoms, obtained from the Monte Carlo models,

multiplied with the sputter yield as a function of bombarding energy, which is computed with an empirical formula [14].

When the Cu atoms are sputtered, they have typical energies of the order of 5–10 eV. They lose this energy, however, rapidly by collisions with the He and Ar gas atoms. This “thermalization process” is simulated with a Monte Carlo algorithm, and this provides the so-called “thermalization profile”, i.e. the number of Cu atoms thermalized as a function of distance from the cathode.

This thermalization profile is used as an input in a fluid model, which treats the thermal Cu atoms, as well as the  $\text{Cu}^+$  ions. This model consists again of two coupled continuity equations (with different production and loss terms) and two transport equations. The production rate of the Cu atoms is given by the flux of sputtered Cu atoms, multiplied by the thermalization profile. The loss of Cu atoms is equal to the production of  $\text{Cu}^+$  ions, and is given by electron impact ionization, Penning ionization with  $\text{He}_m^*$  and with  $\text{Ar}_m^*$  atoms, and asymmetric charge transfer with  $\text{He}^+$  and with  $\text{Ar}^+$  ions. In addition, the Cu atoms can also be lost by deposition at the cell walls, which is taken into account as a boundary condition of the continuity equation, making use of sticking coefficients. Loss of  $\text{Cu}^+$  ions is determined by recombination at the walls, as is the case for all charged species in the model.

Finally, the  $\text{Cu}^+$  ions are also followed with a Monte Carlo model in order to calculate their flux energy distribution at the cathode, since it is expected that the  $\text{Cu}^+$  ions play a non-negligible role in the sputtering process.

All the different models are coupled to each other due to the interaction processes between the various plasma species, and they are solved iteratively until final convergence is reached. This takes typically several days on today's fast computers. More detailed information about this modeling network (e.g. production and loss processes taken into account for the various plasma species, cross-section data, etc.) can be found in [10].

### 3 Experimental set-up

The experiments were performed in a longitudinal HCD, comprising a ring anode and a 5-cm-long cylindrical cathode, made of oxygen-free copper, both having 4-mm inner diameter and 15-mm outer diameter. The two electrodes were isolated from each other by a 0.3-mm-thick quartz ring. They were mounted in a quartz tube with 15-mm inner diameter, so that the discharge could only burn inside the copper cylinder. The two ends of the quartz tube were cut at Brewster's angle for 780.8 nm, so that the HCD tube could be used as a laser tube. The laser resonator was formed by two highly reflecting mirrors for the 740–800 nm spectral range.

The discharge was excited by 3-ms sinusoidal current pulses with 3-Hz pulse repetition rate. In spite of the relatively short length of the tube, laser oscillation could be obtained for the 780.8-nm line. The lasing started at a discharge current of about 1 A ( $\sim 0.16 \text{ A/cm}^2$ ) and the laser power increased linearly with increasing current, exhibiting a tendency to saturate at a discharge current higher than 3 A ( $\sim 0.6 \text{ A/cm}^2$ ). Laser oscillation was obtained only in a mixture of He with 1–10 % Ar concentration and an op-

timum total (i.e. He + Ar) gas pressure of 1.6–2.4 kPa. No lasing could be obtained for Ar concentrations less than 1%, whereas for higher than 10% Ar concentrations, the discharge was very unstable and accurate measurements could not be made.

We measured the laser output power and the on-axis spontaneous emission intensity of copper and helium atomic lines emitted from the whole discharge volume. The measurements were performed at total gas pressure of 2.3 kPa, for 1, 2, 5 and 10% Ar addition. The discharge current was kept at 2.5 A, i.e. below the value at which saturation of the laser power is observed. At these conditions, the measured discharge voltage was around 380 V (slightly varying with He/Ar gas ratio).

## 4 Results and discussion

The calculations were performed for the same longitudinal HCD as that used in the experiment. At one end, an anode ring was assumed at a distance of 0.3 mm, whereas at the other end, a similar hollow cathode was assumed (and the effect on the HCD under study was taken into account in the form of reflecting boundary conditions). Indeed, such a HCD tube is typically used for laser operation in a configuration consisting of several hollow cathodes and anodes in series (e.g. anode–cathode–cathode–anode). The operating conditions (current, voltage and pressure) assumed in the model were the same as those used in the experiment (see above). The gas temperature and cathode wall temperature were actually unknown from experiment, but we assumed a value of 1000 K (see above). The fraction Ar in the gas mixture was varied in a wider range than in the experiment, i.e. between 0% and 50%, to investigate the effect of Ar on the discharge behavior in a systematic way.

Figure 1 shows the calculated density profiles in the longitudinal direction (i.e. as a function of  $z$ -position) and averaged over the radial direction, for the various plasma species at different He/Ar gas ratios and at the conditions mentioned above. The side of the anode ring corresponds to  $z = 0$ , whereas  $z = 5$  cm corresponds to the side of the other HCD tube. The relative contributions of the most important production and loss processes taken into account for these species, calculated by integration over the whole length of the HCD, are summarized in Table 1, for the different He/Ar gas ratios.

### 4.1 Electrons

The electron density profiles (Fig. 1a) are not symmetric in the axial direction, but are characterized by a maximum around  $z = 0.5$ –1 cm, i.e. near the anode side of the HCD tube. This axial non-uniformity is also found in some of the other plasma species densities (see Fig. 1) and is attributed to the characteristic potential distribution found in longitudinal HCDs [15–17]. Indeed, the potential changes significantly in the axial direction, from a slightly positive value (e.g. 10 V) near the anode side, to negative values (e.g. –200 V) near the cathode side. Because the potential at the cathode walls is typically of the order of –300 V, this gives rise to a stronger radial electric field near the anode side, resulting in higher electron energies and more efficient electron impact ioniza-

tion, yielding a higher electron density, compared to the corresponding values at the cathode side.

The electron density clearly increases with the addition of more Ar to the gas mixture. The reason is that Ar has a lower ionization potential than He (i.e. 15.76 eV vs. 24.58 eV); hence, when more Ar is present in the gas mixture, electron impact ionization will be more efficient, leading to a higher electron density.

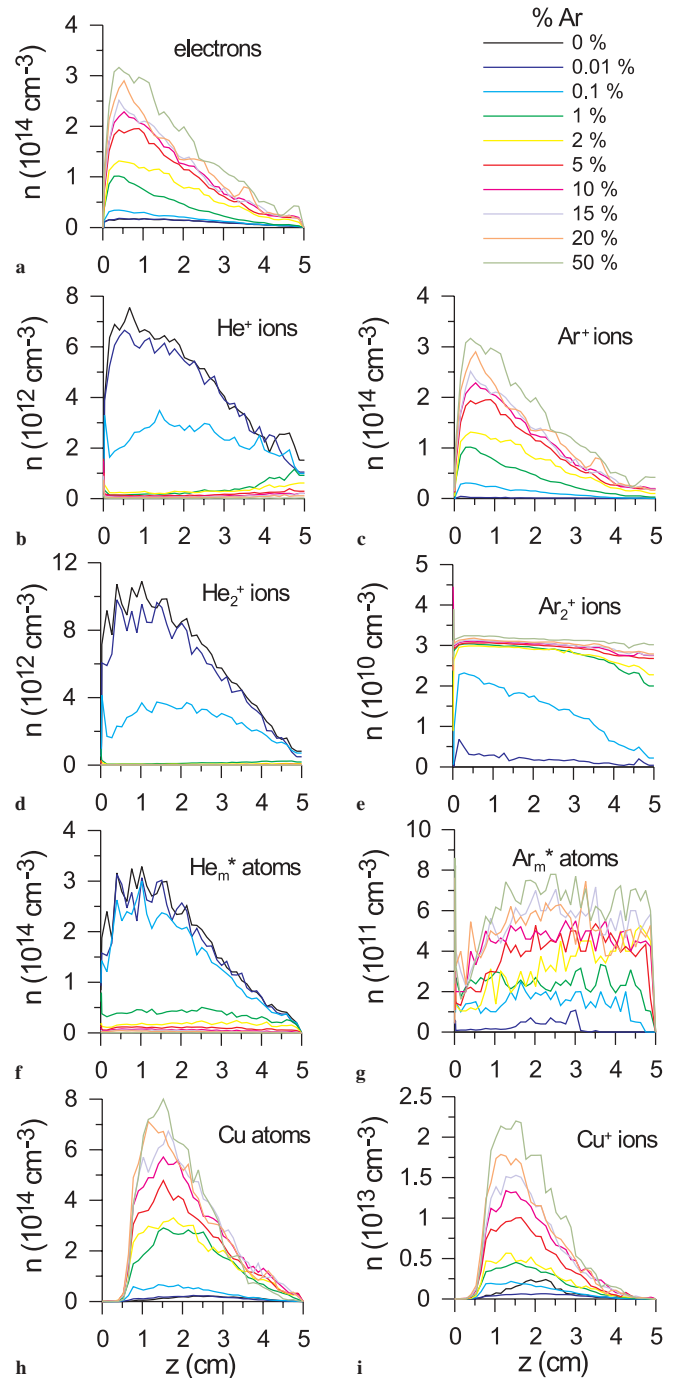


**FIGURE 1** Calculated one-dimensional density profiles in the longitudinal direction (averaged over the radial direction) of the electrons (a),  $\text{He}^+$  ions (b),  $\text{Ar}^+$  ions (c),  $\text{He}_2^+$  ions (d),  $\text{Ar}_2^+$  ions (e),  $\text{He}_m^*$  atoms (f),  $\text{Ar}_m^*$  atoms (g), sputtered Cu atoms (h) and  $\text{Cu}^+$  ions (i), at different Ar concentrations in the He/Ar gas mixture.

% Ar addition:	0%	0.01%	0.1%	1%	2%	5%	10%	15%	20%	50%
<b>Electrons: production:</b>										
Electron impact ionization	62.2	63.1	66.0	73.6	74.1	79.5	81.3	82.3	84.3	92.6
Penning ionization of Ar by He <sub>m</sub> <sup>*</sup>	0	0.2	1.8	11.6	19.4	17.9	17.1	16.4	14.7	7.1
Associative ionization of He	6.2	6.4	7.7	5.1	3.3	2.0	1.5	1.2	1.0	0.3
He <sub>m</sub> <sup>*</sup> -He <sub>m</sub> <sup>*</sup> collisional ionization	31.6	30.3	24.5	9.7	3.2	0.6	0.1	0.1	0.02	~ 10 <sup>-4</sup>
<b>Electrons: loss:</b>										
Recombination with He <sup>+</sup>	50.1	51.4	55.8	49.9	50.1	50.2	43.5	37.9	33.2	14.5
Recombination with Ar <sup>+</sup>	0	~ 0	0.03	2.6	3.9	4.8	6.9	8.3	11.4	27.5
Recombination with He <sub>2</sub> <sup>+</sup>	49.9	48.6	43.9	23.1	13.7	4.3	2.9	2.2	1.8	0.5
Recombination with Ar <sub>2</sub> <sup>+</sup>	0	~ 0	0.1	0.9	1.4	1.6	1.9	2.2	2.5	4.7
Recombination at the walls	0	~ 0	0.2	23.5	30.9	39.1	44.8	49.4	51.1	52.8
<b>He<sup>+</sup> ions: production:</b>										
Electron impact ionization	72.3	74.1	80.0	89.8	97.5	99.4	99.8	99.9	99.97	99.99
He <sub>m</sub> <sup>*</sup> -He <sub>m</sub> <sup>*</sup> collisional ionization	27.7	25.9	20.0	10.2	2.5	0.6	0.2	0.1	0.03	0.01
<b>He<sup>+</sup> ions: loss:</b>										
Recombination with electrons	73.5	73.4	76.2	82.5	84.5	85.6	86.1	87.1	87.6	89.1
Recombination at the walls	26.5	26.6	23.8	17.5	15.5	14.4	13.9	12.9	12.4	10.9
<b>Ar<sup>+</sup> ions: production:</b>										
Electron impact ionization	–	53.9	61.0	65.0	66.1	67.6	68.6	72.4	77.2	91.6
Penning ionization by He <sub>m</sub> <sup>*</sup>	–	46.1	39.0	35.0	33.9	32.4	31.4	27.6	22.8	8.4
<b>Ar<sup>+</sup> ions: loss:</b>										
Recombination with electrons	–	0.3	0.6	5.2	5.8	6.5	8.2	9.0	11.2	19.2
Asymmetric charge transfer	–	0.1	0.3	2.6	3.6	4.5	6.3	6.8	7.1	7.3
Conversion to Ar <sub>2</sub> <sup>+</sup>	–	2.4	2.6	2.9	3.1	3.4	3.6	3.7	4.0	5.6
Recombination at the walls	–	97.2	96.5	89.3	87.5	85.6	81.9	80.5	77.7	67.9
<b>He<sub>2</sub><sup>+</sup> ions: production:</b>										
Associative ionization	21.8	23.2	31.1	42.5	57.4	82.2	93.9	96.7	98.3	99.7
He <sub>m</sub> <sup>*</sup> -He <sub>m</sub> <sup>*</sup> collisional ionization	78.1	76.7	68.8	57.4	42.5	17.6	5.9	3.1	1.5	0.14
Conversion from He <sup>+</sup> ions	0.1	0.1	0.1	0.1	0.1	0.2	0.2	0.2	0.2	0.18
<b>He<sub>2</sub><sup>+</sup> ions: loss:</b>										
Recombination with electrons	88.4	87.9	88.3	91.4	92.0	90.3	89.5	89.0	89.5	89.8
Recombination at the walls	11.6	12.1	11.7	8.6	8.0	9.7	10.5	11.0	10.5	10.2
<b>Ar<sub>2</sub><sup>+</sup> ions: production:</b>										
Conversion from Ar <sup>+</sup> ions	–	98.0	99.9	99.9	99.9	99.9	99.9	99.9	99.9	99.96
Associative ionization	–	1.0	0.05	0.05	0.05	0.05	0.05	0.03	0.03	0.02
Ionization by Ar <sub>m</sub> <sup>*</sup> -Ar <sub>m</sub> <sup>*</sup> collisions	–	1.0	0.05	0.05	0.05	0.05	0.05	0.03	0.03	0.02
<b>Ar<sub>2</sub><sup>+</sup> ions: loss:</b>										
Recombination with electrons	–	91.9	94.8	97.0	97.2	97.5	98.0	98.2	98.4	99.0
Recombination at the walls	–	8.1	5.2	3.0	2.8	2.5	2.0	1.8	1.6	1.0
<b>He<sub>m</sub><sup>*</sup> atoms: production:</b>										
Electron impact excitation	61.9	64.8	66.1	35.2	22.9	18.1	11.6	7.9	7.2	5.4
e <sup>-</sup> /He <sup>+</sup> recombination	31.7	29.7	30.0	60.8	73.0	79.6	86.6	90.6	91.4	93.6
e <sup>-</sup> /He <sub>2</sub> <sup>+</sup> recombination	6.4	5.5	3.9	4.0	4.1	2.3	1.8	1.5	1.4	1.0
<b>He<sub>m</sub><sup>*</sup> atoms: loss:</b>										
Electron impact ionization	19.1	23.2	26.1	75.8	71.6	59.1	46.9	38.9	34.8	20.3
Electron impact de-excitation	3.7	3.9	9.1	5.9	6.5	7.5	6.8	6.5	6.2	4.2
Penning ionization of Cu	0.1	0.1	0.4	0.8	1.1	1.4	1.4	1.1	1.0	0.3
Penning ionization of Ar	0	0.2	1.6	10.3	14.7	26.7	40.3	49.1	54.2	72.0
He <sub>m</sub> <sup>*</sup> -He <sub>m</sub> <sup>*</sup> collisional ionization	68.3	62.3	53.5	2.9	2.2	0.9	0.4	0.3	0.1	0.01
De-excitation at the walls	8.8	10.3	9.3	4.3	3.9	4.4	4.2	4.1	3.7	3.2

<b>Ar<sub>m</sub>* atoms: production:</b>										
Electron impact excitation	–	99.6	99.6	99.8	99.7	99.8	99.8	99.7	99.7	99.7
e <sup>−</sup> -Ar <sup>+</sup> recombination	–	0.4	0.4	0.2	0.3	0.2	0.2	0.3	0.3	0.3
<b>Ar<sub>m</sub>* atoms: loss:</b>										
Electron impact ionization	–	2.1	1.1	1.3	1.0	1.3	1.4	1.4	1.4	1.3
Electron impact excitation	–	91.2	98.1	97.6	98.7	98.5	98.5	98.5	98.5	98.6
De-excitation at the walls	–	6.7	0.8	1.1	0.3	0.2	0.1	0.1	0.1	0.1
<b>Cu atoms: production:</b>										
Sputtering by Ar <sup>+</sup> ions	0	11.1	48.6	66.2	64.1	54.1	44.1	36.2	31.0	16.7
Sputtering by fast Ar atoms	0	0.1	0.5	5.8	12.3	24.2	38.4	47.9	53.7	71.5
Sputtering by Cu <sup>+</sup> ions	20.4	24.0	26.8	23.8	19.5	17.7	14.3	13.2	13.0	10.6
Sputtering by He <sup>+</sup> ions	18.9	15.4	5.7	1.0	1.0	1.0	0.8	0.8	0.7	0.5
Sputtering by fast He atoms	60.7	49.4	18.4	3.2	3.1	3.0	2.4	1.9	1.6	0.7
<b>Cu atoms: loss:</b>										
<b>Cu<sup>+</sup> ions: production:</b>										
Electron impact ionization	62.5	59.8	63.1	65.4	64.0	67.0	62.3	55.4	51.5	34.1
Asym. charge transfer with Ar <sup>+</sup>	0	0.2	2.5	5.3	14.3	20.9	29.2	37.8	42.6	64.1
Asym. charge transfer with He <sup>+</sup>	1.2	1.4	0.8	0.5	1.1	0.7	0.6	0.6	0.4	0.1
Penning ionization by Ar <sub>m</sub> *	0	0.1	0.1	0.2	0.2	0.2	0.3	0.6	0.5	0.9
Penning ionization by He <sub>m</sub> *	36.3	38.5	33.5	28.6	20.4	11.2	7.6	5.6	5.0	0.8
<b>Cu<sup>+</sup> ions: loss:</b>										
Recombination at the walls	100	100	100	100	100	100	100	100	100	100

TABLE 1 Relative contributions (in %) of the different production and loss processes for the various plasma species

Electron impact ionization is indeed the dominant production mechanism for the electrons, and it rises with higher Ar concentration, as appears in Table 1. At very low Ar concentration (< 1%), collisions between two He<sub>m</sub>\* metastable atoms, leading to the ionization of one of the atoms, also play an important role in the production of electrons (of the order of 30%), because the He<sub>m</sub>\* atom density is fairly high at a very low Ar concentration (see further on). Penning ionization of Ar atoms due to He<sub>m</sub>\* metastable atoms also contributes to the production of new electrons, and it reaches a maximum of almost 20% at several-% Ar. Indeed, the addition of more Ar to the gas mixture yields, on the one hand, a higher Ar atom concentration, but, on the other hand, a lower He<sub>m</sub>\* concentration (see below). This gives rise to a maximum in this production rate at several-% Ar.

At very low Ar addition (< 1%), the loss of electrons is almost entirely due to recombination with He<sup>+</sup> ions and He<sub>2</sub><sup>+</sup> ions. However, when more Ar is added to the gas mixture, the He<sup>+</sup> and He<sub>2</sub><sup>+</sup> ion densities gradually drop (see below) and the electrons get primarily lost by electron-ion recombination at the cell walls (using the wall as the third body). Recombination with Ar<sup>+</sup> ions in the plasma itself is not so efficient, because of the lower rate coefficient [10]. Nevertheless, at sufficiently high Ar concentrations, it is a non-negligible loss mechanism for the electrons at the high electrical current typical for laser applications (of the order of a few amperes).

#### 4.2 He and Ar ion densities

Figure 1b–e illustrates the density profiles of the He<sup>+</sup>, Ar<sup>+</sup>, He<sub>2</sub><sup>+</sup> and Ar<sub>2</sub><sup>+</sup> ions at the various He/Ar gas ra-

tios. The Ar<sup>+</sup> ion density profiles (Fig. 1c) increase of course with rising Ar addition, and are almost identical to the electron density profiles (Fig. 1a) for all Ar concentrations studied, except at 0.01% and 0% (in the latter case, the Ar<sup>+</sup> ion density is obviously equal to zero). Because the total electron density in the negative glow region (which fills most of the HCD tube) should be equal to the total ion density, this shows that the Ar<sup>+</sup> ions are the dominant ionic species in the HCD in the He-Ar gas mixture, even at an Ar addition as low as 0.1%. The reason for this has been mentioned above: the Ar<sup>+</sup> ions do not get lost so efficiently by electron-ion recombination, in comparison with the He<sup>+</sup>, He<sub>2</sub><sup>+</sup> and Ar<sub>2</sub><sup>+</sup> ions, due to the lower rate coefficient. Indeed, Table 1 shows that electron-ion recombination in the plasma is of minor importance as a loss mechanism for the Ar<sup>+</sup> ions, whereas it is the dominant loss process for the He<sup>+</sup>, He<sub>2</sub><sup>+</sup> and Ar<sub>2</sub><sup>+</sup> ions. The production of Ar<sup>+</sup> ions is mainly by electron impact ionization (especially at high Ar concentrations), but Penning ionization by He<sub>m</sub>\* atoms plays also an important role, and becomes almost as important as electron impact ionization at very low Ar concentrations (for which the He<sub>m</sub>\* metastable atom density is significant, see below).

The He<sup>+</sup> and He<sub>2</sub><sup>+</sup> ions are only the dominant ionic species at Ar additions below 0.1%, and their densities drop significantly at increasing Ar addition, as appears in Fig. 1b and d. There are two reasons for this: (i) the lower production rate upon Ar addition, as a result of the lower He atom density and the slightly lower electron energy (because the electrons have lost their energy more efficiently by electron impact ionization of Ar); and (ii) the higher loss rate due to efficient recombination with electrons. It appears from our

calculations that the higher loss rate had a more important effect than the lower production rate. This is especially true for the  $\text{He}^+$  ions, which are characterized by a fairly high recombination rate coefficient [10]. At 0 and 0.01% Ar addition, the  $\text{He}_2^+$  ion density is even slightly higher than the  $\text{He}^+$  ion density. This is a little unexpected, since the production rate of  $\text{He}^+$  ions is higher than that for  $\text{He}_2^+$  ions, but it is attributed to the more efficient loss of  $\text{He}^+$  ions. At very low Ar addition, the  $\text{He}^+$  and  $\text{He}_2^+$  ion density profiles are characterized by a maximum at about  $z = 1$  cm (i.e. near the anode side of the HCD tube), in analogy to the electron and  $\text{Ar}^+$  ion density profiles. However, at higher Ar concentrations, the  $\text{He}^+$  and  $\text{He}_2^+$  ion densities reach their maximum at  $z = 5$  cm, i.e. where the electron density is at its minimum, and hence where electron–ion recombination is of minor importance.

Table 1 shows that the production of  $\text{He}^+$  ions is mainly by electron impact ionization, although ionization by collisions of two  $\text{He}_m^*$  atoms is also non-negligible, especially at low Ar concentrations, where the  $\text{He}_m^*$  atom density is quite high. It should be noted that a collision between two  $\text{He}_m^*$  atoms can also lead to the production of  $\text{He}_2^+$  ions by so-called associative ionization, and this process appears to be the dominant production mechanism for the  $\text{He}_2^+$  ions at low Ar concentrations (see Table 1). At high Ar concentrations, in contrast, associative ionization by collisions of He atoms in higher excited levels with He ground-state atoms is the dominant production mechanism for the  $\text{He}_2^+$  ions, as is clear from Table 1. Conversion from  $\text{He}^+$  ions appears to be negligible at all He/Ar gas ratios investigated, due to the low  $\text{He}^+$  ion density.

The  $\text{Ar}_2^+$  ions appear to be negligible at all He/Ar gas ratios studied, as is clear from Fig. 1e, again because of efficient electron–ion recombination (see Table 1). Except at very low Ar concentrations, the  $\text{Ar}_2^+$  ion density is fairly independent of the He/Ar gas ratio. Indeed, more Ar addition results, on the one hand, in more production of  $\text{Ar}_2^+$  ions (by conversion from  $\text{Ar}^+$  ions, which is the dominant production process for the  $\text{Ar}_2^+$  ions, in contrast to the  $\text{He}_2^+$  ions; see Table 1), but on the other hand, in more loss as well, due to recombination with electrons.

#### 4.3 $\text{He}_m^*$ and $\text{Ar}_m^*$ metastable atoms

The density profiles of the  $\text{He}_m^*$  and  $\text{Ar}_m^*$  metastable atoms are illustrated in Fig. 1f and g. The  $\text{He}_m^*$  density (Fig. 1f) reaches a maximum of about  $3 \times 10^{14} \text{ cm}^{-3}$  at about  $z = 1$  cm, at very low Ar concentrations, and it drops considerably upon the addition of more Ar, as was already anticipated above. The reason for this is: (i) the lower production rate (mainly because of the lower He gas density and  $\text{He}^+$  ion density, and also because of the slightly lower electron energy); and (ii) the higher loss rate (see below). The density is in the order of  $5 \times 10^{11} \text{ cm}^{-3}$  at 50% Ar addition, hence almost three orders of magnitude lower than the maximum density at low Ar concentrations. From Table 1, it follows that the  $\text{He}_m^*$  metastable atoms are primarily formed by electron impact excitation at low Ar concentrations, and by electron– $\text{He}^+$  ion recombination at high Ar concentrations (this is indeed the dominant loss mechanism for the  $\text{He}^+$  ions; see above). Loss of the  $\text{He}_m^*$  atoms is mainly attributed to

$\text{He}_m^*$ – $\text{He}_m^*$  collisions (leading to the formation of  $\text{He}^+$  or  $\text{He}_2^+$  ions) at low Ar concentrations (when the  $\text{He}_m^*$  density is fairly high). However, upon the addition of more Ar gas, Penning ionization of the Ar atoms becomes the dominant loss process, and this explains the drop in the  $\text{He}_m^*$  density at higher Ar concentrations. Moreover, electron impact ionization from the metastable levels also appears to be an important loss mechanism, especially at Ar concentrations of several-%.

The  $\text{Ar}_m^*$  metastable density is more uniformly distributed in the axial direction, as is clear from Fig. 1g. The scattering in the curves is simply due to insufficient statistics in the production and loss rates of the  $\text{Ar}_m^*$  atoms, as calculated in the electron Monte Carlo model, even when the latter model was run for several weeks. The  $\text{Ar}_m^*$  density increases with rising Ar addition, as expected. It is of the order of  $5 \times 10^{10} \text{ cm}^{-3}$  at 0.01% Ar concentration, and rises about one order of magnitude (to about  $7 \times 10^{11} \text{ cm}^{-3}$ ) at the He/Ar gas ratio of 50/50. Hence, the  $\text{Ar}_m^*$  metastable density is clearly less sensitive to the He/Ar gas ratio than the  $\text{He}_m^*$  density. We found that the ratio of  $\text{He}_m^*$  and  $\text{Ar}_m^*$  metastable atoms roughly reflects the He/Ar gas ratio, i.e. at 50% Ar addition, the  $\text{He}_m^*$  and  $\text{Ar}_m^*$  metastable densities are of the same order; at 10% Ar addition, the  $\text{Ar}_m^*$  density is about one order of magnitude lower than the  $\text{He}_m^*$  density; at 1% Ar addition, the difference is two orders of magnitude, and so on. This behavior is different from the relative ratios of the  $\text{He}^+$  and  $\text{Ar}^+$  ion densities, where it was found that the  $\text{Ar}^+$  ions are the dominant ionic species, even for Ar concentrations as low as 0.1% (see above). As far as the production and loss of the  $\text{Ar}_m^*$  metastable atoms is concerned, electron impact excitation to the metastable levels was found to be the dominant production mechanism, whereas electron impact excitation from the metastable levels towards higher levels was the dominant loss mechanism at all He/Ar gas ratios investigated.

#### 4.4 Sputtered Cu atoms and $\text{Cu}^+$ ions

The calculated densities of the sputtered Cu atoms and the corresponding  $\text{Cu}^+$  ions increase with the addition of more Ar to the gas mixture, as can be seen in Fig. 1h and i. This is as expected because Ar is known to be added to the gas mixture to promote sputtering. A rise in the Cu atom concentration vs. %Ar addition was also experimentally observed [8].

It follows indeed from Table 1 that, except at very low Ar concentrations, most of the Cu sputtering is due to  $\text{Ar}^+$  ions and fast Ar atoms. The latter are created from collisions of the fast  $\text{Ar}^+$  ions with Ar gas atoms on their way towards the cathode. Obviously, more fast Ar atoms are created when more Ar gas is present in the gas mixture, which explains the dominant contribution of fast Ar atoms to the Cu sputtering at the highest Ar concentrations. The role of  $\text{He}^+$  ions and fast He atoms is only non-negligible at very low Ar additions (< a few %), but this is not because of the increasing efficiency of the He species, but simply due to the low  $\text{Ar}^+$  ion and fast Ar atom fluxes bombarding the cathode. The  $\text{Cu}^+$  ions, in contrast, play a quite important role in the sputtering process (so-called “self-sputtering”), as is clear from Table 1.

The loss of Cu atoms is due to various ionization mechanisms, as well as deposition at the cell walls (taken into

account as a boundary condition in the continuity equation, using a sticking coefficient). The latter loss mechanism is not, however, explicitly accounted for in the table because of considerable uncertainties in the sticking coefficient. The relative contributions of the different ionization mechanisms are, however, of more importance, because they also determine the production of  $\text{Cu}^+$  ions. Electron impact ionization appears to be the dominant ionization mechanism, but upon the addition of more Ar gas, asymmetric charge transfer with  $\text{Ar}^+$  ions becomes increasingly important, and it seems to even become dominant at the highest Ar concentration investigated. This trend is as expected, because of the increasing density of  $\text{Ar}^+$  ions. Similarly, the role of Penning ionization by  $\text{He}_m^*$  metastable atoms rises with lower Ar gas concentrations because of the increasing density of the  $\text{He}_m^*$  atoms. Penning ionization by  $\text{Ar}_m^*$  atoms and asymmetric charge transfer by  $\text{He}^+$  ions, in contrast, are found to be of minor importance for the ionization of Cu at all He/Ar gas ratios investigated. This was expected because of the low  $\text{Ar}_m^*$  and  $\text{He}^+$  densities (see Fig. 1d and i). Note that the exact values of these calculated relative contributions should be considered with caution because of the uncertainties in the rate coefficients for both Penning ionization and asymmetric charge transfer. Nevertheless, the general trend is expected to be correctly predicted. The degree of ionization of Cu was calculated to be about 1–2 % at all He/Ar gas ratios investigated. Finally, Table 1 shows that the loss of  $\text{Cu}^+$  ions is entirely attributed to electron–ion recombination at the cell walls, which was the only loss mechanism taken into account for these species.

#### 4.5 Effect of the He/Ar gas ratio on the laser operation – comparison with experiment

The above result regarding the minor importance of asymmetric charge transfer of Cu atoms with  $\text{He}^+$  ions as an ionization mechanism for the Cu atoms has some important consequences for the laser efficiency of the He–Ar– $\text{Cu}^+$  IR HCD laser. Indeed, this process is known to be the population mechanism of the upper laser level; hence, it determines the degree of population inversion, and therefore the laser power. It can be deduced from Table 1 that only about 1% or less of the  $\text{Cu}^+$  ions will be excited to the  $3d^9 6s^3 D_3$  level, which is the upper laser level for the 780.78-nm laser line. This outcome suggests that the laser power of the He–Ar– $\text{Cu}^+$  IR HCD laser could be improved when asymmetric charge transfer between Cu atoms and  $\text{He}^+$  ions becomes more efficient.

Figure 2 shows the calculated Cu atom density (small dashed line, first left axis) and the  $\text{He}^+$  ion density (wider dashed line, second left axis), both integrated over the axial and radial directions (hence over the entire discharge tube), as a function of the Ar addition. Also shown is the product of both values (solid line, right axis), which determines the production rate of the  $\text{Cu}^+$  ions in the upper laser level and hence the laser output power (assuming that the population of the lower laser level is not sensitive to the Ar addition).

Upon addition of more Ar gas, the calculated Cu atom density rises as a result of enhanced sputtering (see also above), whereas the  $\text{He}^+$  ion density drops, due to the lower production rate and the increased loss by electron–ion recombination (see also above). As a result of these two opposite

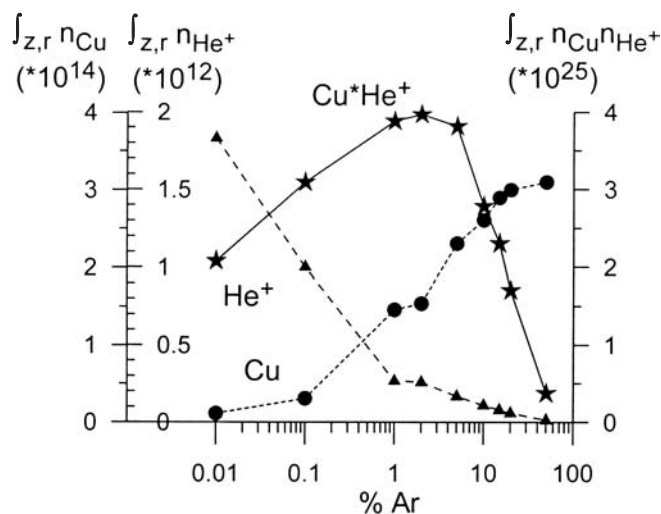


FIGURE 2 Calculated Cu atom density (small dashed line, first left axis),  $\text{He}^+$  ion density (wider dashed line, second left axis) and product of both (solid line, right axis), as a function of Ar concentration in the gas mixture. Note that the densities are integrated over the entire discharge tube (both radial and axial directions)

trends, the product of both densities reaches a maximum at an intermediate Ar concentration of 1–5 %, as follows from Fig. 2. Hence, this suggests that the production rate of the  $\text{Cu}^+$  ions in the upper laser level, and therefore probably also the laser output power, is at a maximum at 1–5 % Ar addition.

To check this calculation result, Fig. 3 shows the measured optical emission intensities of a Cu I line (small dashed line, first left axis) and a He I line (wider dashed line, second left axis), as well as the measured laser output power (solid line, right axis), as a function of Ar concentration. The densities of Cu atoms and  $\text{He}^+$  ions could not be measured in the present experiment, but the above optical emission intensities should exhibit the same trend as the densities. It is clear from Fig. 3 that the Cu I line intensity increases and the He I line intensity drops with increasing Ar addition, which is in correspondence

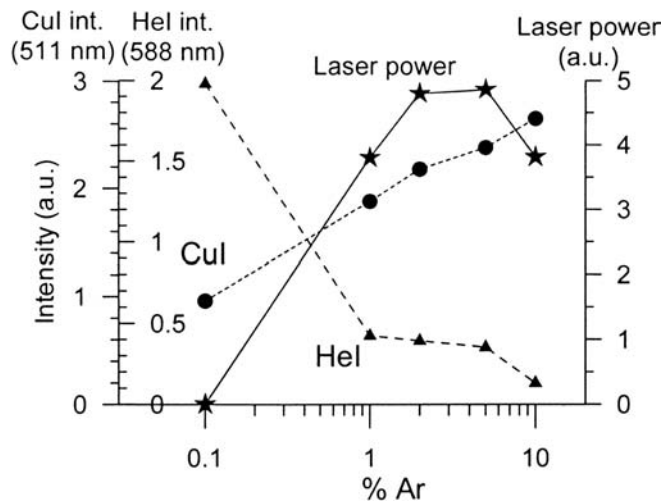


FIGURE 3 Measured Cu I 511-nm line intensity (small dashed line, first left axis), He I 588-nm line intensity (wider dashed line, second left axis) and laser output power (solid line, right axis), as a function of Ar concentration in the gas mixture

with the above calculation results for the densities. Moreover, the measured laser output power reaches a maximum at 2–5 % Ar addition. This is also in reasonable agreement with the theoretical predictions, certainly if one realizes that both model and experiment are subject to considerable uncertainties (i.e. uncertainties in the input data for the model, and the low laser intensities in the experiment, because of the short laser tube). This illustrates that the correct processes are described in our model for the He-Ar-Cu<sup>+</sup> IR HCD laser.

## 5 Conclusion

A comprehensive modeling network developed for a He-Ar-Cu<sup>+</sup> IR HCD laser is used to investigate the effect of the He/Ar gas ratio on the discharge properties and on the laser operation. It is found that the Ar concentration has a quite significant effect on the plasma characteristics. Upon the addition of more Ar gas, the densities of electrons, Ar<sup>+</sup> ions, Ar<sub>m</sub><sup>\*</sup> metastable atoms, sputtered Cu atoms and Cu<sup>+</sup> ions increase, whereas the densities of the He<sup>+</sup> ions, He<sub>2</sub><sup>+</sup> ions and He<sub>m</sub><sup>\*</sup> metastable atoms drop significantly. The rise in electron density is attributed to increased electron impact ionization efficiency, because Ar has a lower ionization potential than He. The rise in densities of the Ar species is logical when more Ar is present in the gas mixture. The increase in sputtered Cu atom and Cu<sup>+</sup> ion densities is due to the enhanced sputtering by Ar<sup>+</sup> ions and fast Ar atoms. The drop in He<sup>+</sup> and He<sub>2</sub><sup>+</sup> ion densities is explained by the lower production rate and the more efficient electron–ion recombination at higher Ar concentrations (and hence higher electron densities), whereas the drop in the He<sub>m</sub><sup>\*</sup> atom density is attributed to the lower production rate and the higher loss rate due to Penning ionization of the Ar gas atoms.

As the He<sup>+</sup> ion density decreases and the sputtered Cu atom density increases when more Ar is added to the gas mixture, the product of both appears to reach a maximum at 1–5 % Ar addition. As this product determines the production rate of the upper laser level (by asymmetric charge transfer), our model predicts that this He/Ar gas ratio also yields opti-

imum laser output power (assuming that the production rate of the lower laser level is not affected by the He/Ar gas ratio). This outcome is in reasonable agreement with the experimental results, which exhibit a maximum laser output power at 2–5 %. This shows that our model describes rather well the important plasma processes taking place in the He-Ar-Cu<sup>+</sup> IR HCD laser.

**ACKNOWLEDGEMENTS** A. Bogaerts is indebted to the Flemish Fund for Scientific Research (FWO) for financial support. The authors also acknowledge the financial support from an FWO “New Research Project”, from a Joint Research Project between the Bulgarian Academy of Sciences (BAS) and the FWO, and from NATO’s Scientific Affairs Division in the framework of the Science for Peace Programme, Project No. NATO SfP-971989 ‘SfP-Excimer Laser’.

## REFERENCES

- 1 D.C. Gerstenberger, R. Solanki, G.J. Collins: *IEEE J. Quant. Electron.* **QE-16**, 820 (1980)
- 2 I.G. Ivanov, E.L. Latush, M.F. Sem: *Metal Vapor Ion Lasers: Kinetic Processes and Gas Discharges* (Wiley, Chichester 1996)
- 3 L. Csillag, M. Janossy, K. Rozsa, T. Salamon: *Phys. Lett. A* **50**, 13 (1974)
- 4 H.J. Eichler, H.J. Koch, J. Salk, G. Schäfer: *IEEE J. Quant. Electron.* **QE-15**, 908 (1979)
- 5 J.R. McNeil, G.J. Collins, K.B. Persson, D.L. Franzen: *Appl. Phys. Lett.* **27**, 595 (1975)
- 6 K.A. Peard, Z. Donko, K. Rozsa, L. Szalai, R.C. Tobin: *IEEE J. Quant. Electron.* **QE-30**, 2157 (1994)
- 7 R.R. Arslanbekov, R.C. Tobin, A.A. Kudryatsev: *J. Appl. Phys.* **81**, 554 (1997)
- 8 K.A. Peard, K. Rozsa, R.C. Tobin: *J. Phys. D: Appl. Phys.* **27**, 219 (1994)
- 9 H.J. Eichler, W. Wittwer: *J. Appl. Phys.* **51**, 80 (1980)
- 10 A. Bogaerts, R. Gijbels: *J. Appl. Phys.* **92**, 6408 (2002)
- 11 A. Bogaerts, R. Gijbels, V.V. Serikov: *J. Appl. Phys.* **87**, 8334 (2000)
- 12 R. Deloche, P. Monchicourt, M. Cheret, F. Lambert: *Phys. Rev. A* **13**, 1140 (1976)
- 13 K. Kutasi, P. Hartmann, Z. Donko: *J. Phys. D: Appl. Phys.* **34**, 3368 (2001)
- 14 N. Matsunami, Y. Yamamura, Y. Itikawa, N. Itoh, Y. Kazumata, S. Miyagawa, K. Morita, R. Shimizu, H. Tawara: *At. Data Nucl. Data Tables* **31**, 1 (1984)
- 15 A. Bogaerts, M. Grozeva: *Appl. Phys. B* **75**, 731 (2002)
- 16 J. Myzeraczyk: *Acta Phys. Hung.* **54**, 71 (1983)
- 17 J. Myzeraczyk: *J. Phys. D: Appl. Phys.* **20**, 429 (1987)